

Soft-UV Photolithography using Self-Assembled Monolayers

Kevin Critchley,[†] Lixin Zhang,[‡] Hitoshi Fukushima,[§] Masaya Ishida,[⊥] Tatsuya Shimoda,[§] Richard J. Bushby,[‡] and Stephen D. Evans^{*,†}

School of Physics and Astronomy, University of Leeds, Leeds LS2 9JT, UK, Self-Organizing Molecular Systems (SOMS) Centre, University of Leeds, Leeds LS2 9JT, UK, I/O group/Technology Platform Research Centre—Seiko Epson Corporation, Fujimi Plant: 281 Fujimi, Fujimi-machi, Suwa-gun, Nagano-ken 399-0293, Japan, and Cambridge Research Laboratory of Epson, 9A Science Park, Milton Rd, Cambridge CB4 0FE, UK

Received: May 18, 2006; In Final Form: July 5, 2006

We report thiol-on-gold self-assembled monolayers (SAMs) that can be photodeprotected using soft UV irradiation ($\lambda = 365$ nm) to yield CO₂H functionalized surfaces complementing those reported previously, which yielded NH₂ functionalized surfaces. The photolysis of these SAMs were monitored using a combination of surface sensitive techniques. In the SAM environment the photodeprotection yields are lower than those obtained for equivalent reactions in dilute solution. The protected carboxylic acids SAMs are shown to have a low yield $\sim 50\%$ due to competing photoreduction reactions of the nitro group. The results from infrared studies show that, as the photolysis progresses, the long chain protected residues reorganize and shield the functional COOH groups, thereby reducing the hydrophilic character of the surface.

1. Introduction

The photopatterning of self-assembled monolayers (SAMs) on silicon and gold, using short wavelength ultraviolet (UV) light, was first reported in the early 1990s.^{1–7} In the case of the alkanethiol derivatives on noble metal surfaces, the alkanethiolate groups can be photooxidized by UV light (≤ 252 nm), leading to sulfoxides and sulfonates that can be readily displaced by other thiol derivatives in solution.^{4,8,9} Recent studies have shown this process is strongly dependent on the packing within the alkanethiolate SAMs.^{8,9} Organosilanes also require deep UV light to instigate photocleavage of the Si–C or C–C bonds.^{2,10} The efficiency of these photoreactions are dependent on the molecular structure, and it is likely that following photodegradation the surface is left with a variety of chemically modified groups.^{3,10–15} In our work, we have elected to use longer wavelength UV light (365 nm),¹⁶ the advantages of this are (1) It provides better control over the photochemistry and should produce better defined surfaces; (2) It is compatible with conventional photolithographic techniques; and (3) This wavelength of light is compatible with biological molecules, therefore permitting multiple exposures without degradation.¹⁷

In this paper, we report SAMs that can be modified using soft UV irradiation to yield CO₂H functionalized surfaces (SAM1 and SAM2, Figure 1). These complement SAMs that we reported in a previous paper which yielded NH₂ functionalized surfaces (SAM3, Figure 1).¹⁶ The creation of the CO₂H or NH₂ functional groups relies on the photocleavage of an *ortho*-nitrobenzyl moiety. Most, but not all,¹⁸ previous attempts to translate *ortho*-nitrobenzyl photochemistry from dilute solution to the SAM environment have concentrated on silane-on-

SiO₂ SAMs.^{17,19–26} Whitesides et al. recently demonstrated that similar systems could be used to create multiple component surfaces using “deep” and soft UV irradiation.¹⁸ Here, however, we demonstrate that the hydrophobicity of surfaces can be controlled using such SAMs and that the reaction is more complex than that occurring in solution.

The design of SAM2 is based simply on the protection of the CO₂H as the *ortho*-nitrobenzyl ester where a key step in the photodeprotection is the fragmentation of cyclic intermediate **4a** (Figure 2).^{27,28} For SAM3, the corresponding intermediate is **4b** and the equivalent fragmentation involves a co-elimination of carbon dioxide. These heterolytic fragmentation pathways can be extended in many different ways and in the case of SAM1 the fragmentation of the intermediate **4c** leads to co-elimination of both carbon dioxide and formaldehyde. This proves just as effective as the fragmentation of **4a**. The generic nature of this *ortho*-nitrobenzyl photodeprotection chemistry means that many other variations of this type are possible as are variations in the leaving group. However, as will be seen, the weaknesses of *ortho*-nitrobenzyl based systems are also intrinsic in nature. Taken together, SAM1–SAM3 give us the ability to photopattern gold surfaces either with CO₂H or NH₂ functional groups, but the reactions are not as clean as equivalent photoreactions in dilute solution.^{17,19} In the SAM environment there is a significant side-reaction that leaves some of the protecting group “permanently” bound to the surface. In the case of SAM2, this is shown to be the result of a competitive photoreduction of the *ortho*-nitro group. The side reactions occur in all of the systems we have studied¹⁶ and lead to surfaces that are more hydrophobic than expected. A detailed IR study of SAM2 shows that the long chain protected moieties reorganize as the photoreaction proceeds.

2. Experimental Section

2.1. Materials. Dichloromethane 99.9% (DCM), hydrogen peroxide (27.5 wt. %), 4,4'-Dithiodibutyric acid, $-\text{[S(CH}_2\text{)}_3\text{-CO}_2\text{H]}_2$ (hereafter known as DTBA), were used as received from

* Corresponding author phone: +44 113 343 3852; fax: +44 113 343 3900; e-mail: s.d.evans@leeds.ac.uk.

[†] School of Physics and Astronomy, University of Leeds.

[‡] Self-Organizing Molecular Systems (SOMS) Centre, University of Leeds.

[§] Seiko Epson Corporation.

[⊥] Cambridge Research Laboratory of Epson.

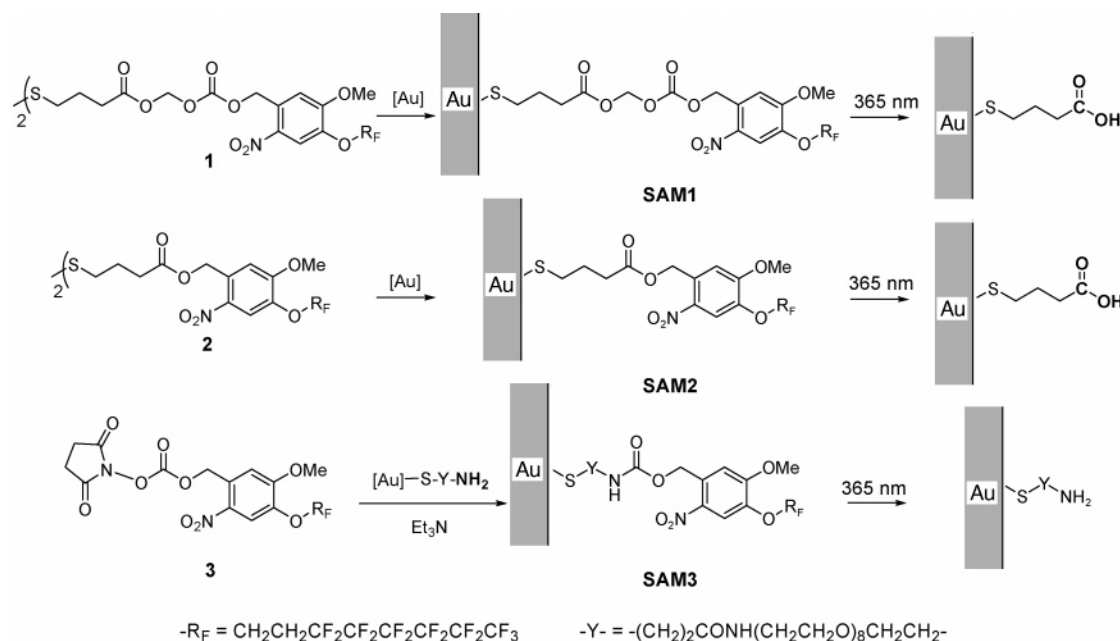


Figure 1. Reagents **1**, **2**, and **3** are used in the formation of SAM1, SAM2, and SAM3, respectively. Photolysis of SAM1 or SAM2 using 365 nm UV light generates CO₂H functionalized surfaces, whereas SAM3 gives an NH₂ functionalized surface.

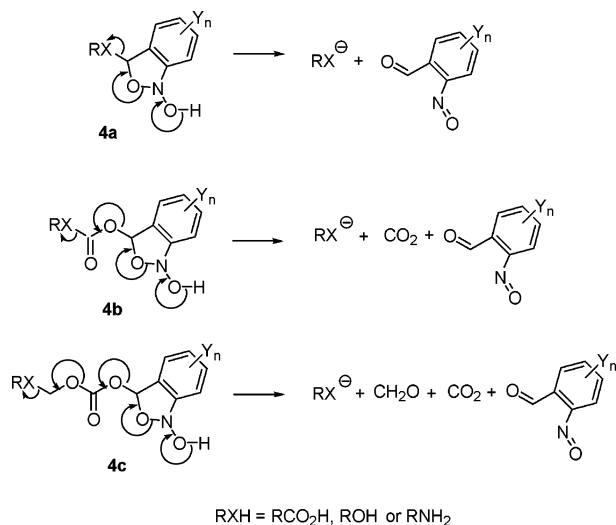


Figure 2. Intermediates in the photolysis of ortho-nitrobenzyl compounds showing the relationship between the likely photofragmentation pathways (see text).

Sigma-Aldrich. Sulfuric acid (98%) was supplied by Fisher Scientific. Glass microscope slides (thickness of 0.8 mm) were purchased from Agar and were cut approximately three-quarters of the original length. Millipore Milli-Q water with a resistivity better than 18.1 MΩcm was used throughout. High purity (99.99%) temper annealed gold wire (0.5 mm diameter) was supplied by Advent. The syntheses of compounds **1** and **2** are summarized in Figure 3; further details of the synthesis are given in the Supporting Information.^{29–32}

2.2. Substrate Preparation. The glass microscope slides were first cleaned by ultrasonication for 15 min in a 10% solution of Decon90 in Milli-Q water. Each slide was rinsed 10 times in Milli-Q water and then dried under a stream of nitrogen. The samples were ultrasonicated in dichloromethane for 15 min, removed and dried, rinsed under Milli-Q water, and immersed in piranha solution (70:30, v/v, H₂SO₄: H₂O₂) for 10 min. *Caution: piranha solution reacts violently with organic materials and should be treated with great care.* The substrates were then rinsed in Milli-Q-grade water, dried under nitrogen,

and placed in an Edwards Auto 306 thermal evaporator. A 200 nm gold layer was thermally deposited (0.1 nm s⁻¹) onto a chromium adhesion layer (5 nm), at a base pressure of approximately 1 × 10⁻⁶ mbar. The gold-coated samples were cleaned immediately prior to use by placing them in freshly prepared piranha solution for 1–2 min, followed by a rinse with Milli-Q water.

2.3. SAM Adsorption. SAM1 and SAM2 were formed by immersing the gold-coated slides in 0.5 mM solutions of the corresponding disulfide (**1** or **2**) in DCM for 16 h, at 23 °C (DCM was used to enhance the solubility of **1** and **2**). Mixed SAMs were formed from mixed solutions of the disulfide **2** and DTBA. Once again, a combined solution concentration of 0.5 mM was employed and they were left to form for 16 h at 23 °C. The relative molar concentrations employed were (**2**:DTBA) 25:100, 50:100, 75:100, 85:100, and 95:100. All of the SAMs were removed from solution, rinsed with DCM, dried with a nitrogen stream, rinsed with Milli-Q grade water, and again dried.

2.4. UV Irradiation of SAMs. A 365 nm UV lamp (Blak-Ray Model B 100 AP) with a nominal power (at the sample) of 7 mWcm⁻² was used to irradiate the samples, in air, for 3600 s unless stated otherwise. After the UV irradiation, samples were rinsed with DCM, followed by Milli-Q water, and finally dried under a stream of nitrogen. The emission spectra of the lamp displayed three lines, 309, 331, and 365 nm, with relative integrated intensities of 0.005: 0.03: 1, respectively.

2.5. Wetting Measurements. Contact angles were measured using a First-Ten-Angstrom 2000 goniometer under ambient conditions. Milli-Q water droplets were advanced and receded across the surface from a microsyringe needle. Images of at least six advancing and receding droplets were analyzed on both sides of each droplet to give a minimum of six values per surface.

2.6. X-ray Photoelectron Spectroscopy. Spectra were obtained using a Thermo Electron Corporation ESCA Lab 250 with a chamber pressure maintained below 1 × 10⁻⁹ mbar during acquisition. A monochromated Al Kα X-ray source (15 kV 150 W) irradiated the samples, with a spot diameter of approximately 0.5 mm. The spectrometer was operated in Large Area XL magnetic lens mode using pass energies of 150 and

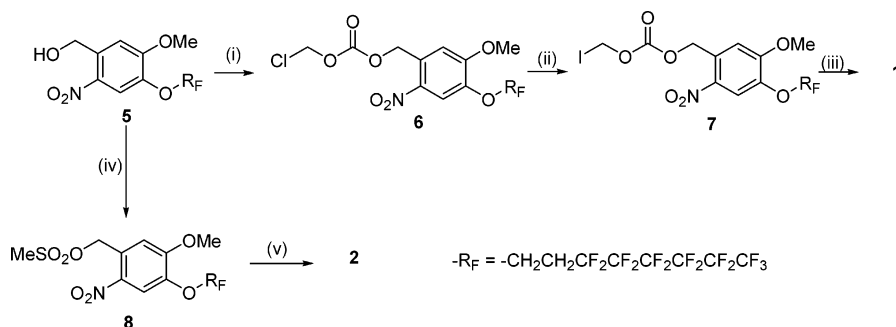


Figure 3. Syntheses of compounds **1** and **2**. Reagents (i) $\text{ClCH}_2\text{OCOCl}/N\text{-methylmorpholine}/51\%$ ²⁹ (ii) $\text{I}_2/\text{acetone}/47\%$ ³⁰ (iii) $-\text{[S}(\text{CH}_2)_3\text{CO}_2\text{Cs}]_2/\text{DMF}/51\%$ ³¹ (iv) $\text{MeSO}_2\text{Cl}/\text{Et}_3\text{N}/\text{THF}/95\%$ ³² (v) $-\text{[S}(\text{CH}_2)_3\text{CO}_2\text{Cs}]_2/\text{DMF}/47\%$. The synthesis of the starting material **5** is detailed in ref 16.

TABLE 1: Surface Properties of SAM1, SAM2, and DTBA SAMs

SAM	water contact angles/degrees		ellipsometric thickness/Å	expected thickness/Å
	θ_A	θ_R		
SAM1	117 ± 1	108 ± 1	17.6 ± 0.4	22.3
SAM2	112 ± 1	97 ± 2	14.3 ± 0.4	15.4
SAM3 ref. ¹⁶	112 ± 1	74 ± 1	30 ± 2	26
SAM1 after UV	87 ± 1	63 ± 1	6.0 ± 0.8	>5.6
SAM2 after UV	91 ± 1	66 ± 1	6.2 ± 0.2	>5.6
SAM3 after UV ref. ¹⁶	64 ± 1	30 ± 1	26 ± 1	>26
DTBA SAM	<5	<5		5.6

20 eV for survey and detailed scans, respectively. The spectra were obtained with an electron takeoff angle of 90° . High-resolution spectra were fitted using Advantage (Thermo VG software package) peak fitting algorithms. All spectra have been normalized to the Au $4f_{7/2}$ peak.

2.7. Ellipsometry. A Jobin-Yvon UVISSEL spectroscopic ellipsometer was used to measure the thickness of the SAMs. The wavelength was varied between 300 and 800 nm, in steps of 15 nm. DeltaPsi2 software was used to model and fit the acquired data assuming a simple three-layer system. Values for the base layer (gold support) were obtained from a freshly cleaned gold substrate. The SAM was modeled as a transparent thin film using the Cauchy approximation, $n(\lambda) = A + B \cdot 10^4 / \lambda^2 + C \cdot 10^9 / \lambda^4$ and $k(\lambda) = 0$.³³ Where λ is the wavelength in units of nanometers and A, B, and C are the Cauchy parameters dependent on optical properties of the material. Parameter, A, was restricted to a value of 1.38 and parameters B and C were allowed to vary between 0 and 1 nm^2 and $0\text{--}0.2 \text{ nm}^4$ respectively. The ambient air was assumed to have $n = 1$ and $k = 0$. At least six ellipsometric measurements were made per sample (and on more than one sample of each type).

2.8. Time-of-Flight SIMS (ToFSIMS). ToFSIMS spectra were acquired using a PHI 7000 instrument equipped with a cesium ion source. Spectra were acquired from nonirradiated and UV irradiated samples. The analysis area was $300 \mu\text{m} \times 300 \mu\text{m}$.

3. Results and Discussion

3.1. Synthesis. In our previous work, the protection step was performed in-situ using a triethylamine catalyzed reaction of an N-hydroxysuccinimoyl carbamate reagent with the amine-functionalized SAM (Figure 1).¹⁶ The advantage of this derivatization in situ is that the reagent can be used to protect any amine functionalized surface, including both alkanethiols on gold and organosilanes on silicon. However, the reaction between the surface amine groups and reagent was not wholly clean¹⁶ and so, in this study, we have chosen to form photoreactive SAMs directly from the disulfide derivatives **1** and **2** in which the *ortho*-nitrobenzyl protecting group is already in place. This

reduces the versatility of the reagents and limits the chemistry to ‘thiol-on-gold’ systems, but guarantees a chemically homogeneous surface before the photoprotection. The syntheses of the disulfides were straightforward, and the routes used are summarized in Figure 3. Further details are given in the Supporting Information.

3.2. Characterization of SAM1 and SAM2. The SAMs were formed as described in the Experimental Section, and the surface properties are summarized in Table 1. The advancing and receding water contact angles of SAM1 are comparable to long-chain semi-fluorinated SAMs.^{34–37} These large contact angles indicate a high density of $-\text{CF}_3$ groups at the monolayer/air interface. Furthermore, the small hysteresis suggests that SAM1 modified surfaces are chemically homogeneous. SAM2 had slightly lower contact angles than SAM1 and a larger hysteresis suggesting a lower packing density and/or an increased level of disorder. In both cases, the hydrophobicity was significantly greater than SAM3 (described in our previous work).¹⁶

The SAM thicknesses were determined by spectroscopic ellipsometry (Table 1), assuming the refractive indices of SAM1 and SAM2 to be similar to fluorocarbon materials, i.e., $n = 1.38$,³⁸ using a refractive index of 1.45 reduces the modeled thickness values by 12%. Molecular modeling (MOPAC) of single molecules of **1** and **2**, were performed in order to estimate the molecular thicknesses of the respective SAMs. If one assumes that the hydrocarbon chains at the base of SAMs are orientated at 30° with respect to the normal of the gold surface, then the expected thicknesses of SAM1 and SAM2 are estimated to be 22 and 15 Å, respectively. SAM1 was found to be thinner than the estimated thickness, while SAM2 had a similar thickness to that predicted. However, comparisons should be viewed with caution since the compounds were modeled as single molecules in a vacuum and the conformation of the molecules in a SAM may differ. Following irradiation the remaining hydrocarbons chains were modeled assuming a refractive index of 1.45.

Figure 4a shows the X-ray photoelectron spectra of the C 1s region of SAM1. The bands located at 293.5, 291.3, and 290.5 eV are assigned to CF_3 , CF_2 , and CF_2CH_2 species, respectively.^{39–41}

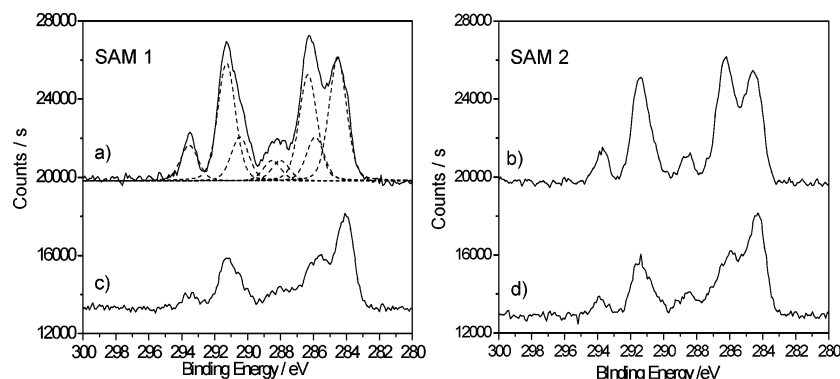


Figure 4. X-ray photoelectron spectra of the C 1s region; (a) SAM1 on Au; (b) SAM2 on Au; (c) SAM1 after 3600 s of UV (365 nm, 7 mW/cm²) irradiation.; (d) SAM2 after 3600 s of UV (365 nm, 7 mW/cm²) irradiation. Spectra (a) shows an example of how these data were fitted to Pseudo-Voigt peak functions (FWHM = 1.2 eV and a Lorentzian to Gaussian mix of 3:7). The spectra have been translated vertically for display purposes.

TABLE 2: Summary of FT-IR Spectrum Peak Assignments for SAM1 and SAM2

wavenumber/cm ⁻¹	assignment	description
1774	$\nu(\text{OCOO})$	C=O stretch of the -OCOO- group
1741	$\nu(\text{COO})$	C=O stretch of the -COO- group
1533	$\nu_a(\text{NO}_2)$	asymmetric stretch aromatic NO ₂ ⁴⁴
1289	$\nu(\text{OCH}_3)$	asymmetric aryl C-O stretch ⁴⁴
1251	$\nu_a(\text{CF}_2)$, $r(\text{CF}_2)$	asymmetric stretch perpendicular to the axis ⁴⁵⁻⁴⁸
1215	$\delta(\text{CCC})$, $\nu(\text{CC})$	CCC bend and CC stretch of the fluorocarbon chain (parallel to the axis) ⁴⁵⁻⁴⁸
1148	$\nu_s(\text{CF}_2)$, $\delta(\text{CF}_2)$	symmetric CF2 stretch and CF2 scissors (perpendicular to the axis) ⁴⁵⁻⁴⁸

The bands at 288.5 and 288.0 eV are associated with C=O groups.³⁹ The peak at 286.3 eV is assigned to the -C-O species and the bands at 285.9 and 284.5 eV are associated with the hydrocarbons CH₂CF₂ and CH₂/CH_{arom}, respectively.^{39,41} The XPS-determined ratio of fluorinated to nonfluorinated carbon species is 0.58, which is larger than the 0.38 predicted from the composition of the material used to form SAM1. The difference is due to photoelectron attenuation effects from the upper portions of the SAM molecules.^{42,43} The C 1s spectrum of SAM2 is very similar to SAM1 (Figure 4b), however, for SAM2, the XPS-determined ratio of fluorinated to nonfluorinated carbons is 0.47. This is slightly larger than the ratio of 0.43 predicted by the composition of SAM2; however, the difference in the “expected” to “observed” ratios is smaller for SAM2 than for SAM1, suggesting that SAM2 was thinner and that the molecules in the SAM are less densely packed.

The FT-IR spectra of SAM1 and SAM2 are shown in Figures 5a and b, respectively. The main peaks are summarized in Table 2. In both systems, the most intense peak was found at 1533 cm⁻¹ and is associated with the aromatic-nitro asymmetric stretch.⁴⁴ The symmetric NO₂ stretch will be located between 1337 and 1360 cm⁻¹; however, this peak is masked by other vibrations.⁴⁴ Peaks found between 1100 and 1251 cm⁻¹ have previously been assigned to vibrations in the fluorocarbon chain.⁴⁵⁻⁴⁸ The aromatic methoxy vibration occurs close to 1289 cm⁻¹.⁴⁴ The most significant difference between the spectra of the two SAMs is the presence of an intense band at 1774 cm⁻¹ associated with the OCOO vibration in the case of SAM1.

3.3. Mixed SAMs of Compound 2 and DTBA. If the photolysis of SAM2 was clean and had a reaction yield of 100%, the surface produced would effectively be equivalent to SAMs formed from molecules of DTBA (-[S(CH₂)₃CO₂H]₂), with some small variation due to packing differences. Thus by using mixtures of 2 and DTBA, we can create mixed SAMs that mimic the various stages of the ideal photolysis. Mixed SAMs were produced by adsorption from DCM and the resultant surfaces were analyzed using XPS. The relationship between solution concentration and surface concentration was nonlinear, and the

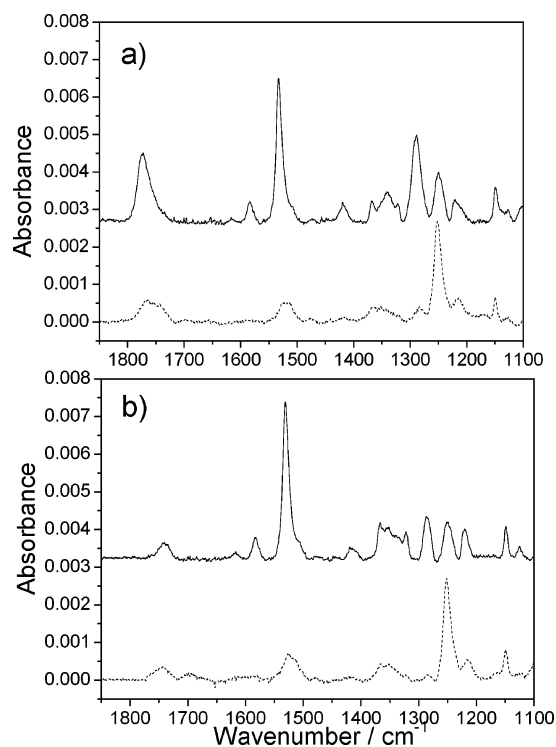


Figure 5. Fourier transform infrared reflectance spectra of (a) SAM1 and (b) SAM2. The solid and dashed lines represent before and after exposure to UV (365 nm, 7 mW/cm²) irradiation, for 60 min, respectively. The spectra have been translated vertically for display purposes.

DTBA compound was found to be the dominating adsorbent under the conditions described (Supporting Information).

The advancing water contact angles measured on these “mixed SAMs” are displayed in Figure 6 (right axis). The SAM formed from 100% DTBA solution produced extremely hydrophilic surfaces, with water contact angles similar to those obtained for other carboxylic acid functionalized SAMs.^{35,49} The FT-IR spectrum acquired for each mixed SAM (Figure 6) shows two main bands associated with the asymmetric nitro

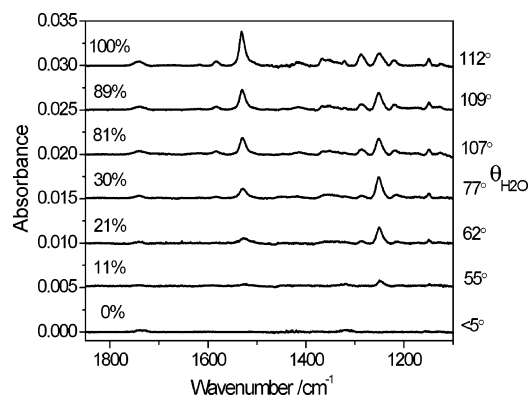


Figure 6. FT-IR spectra of the “mixed” monolayers of **2** and DTBA. The percentages represent the surface coverage of **2** as determined by XPS. The corresponding advancing water contact angles are displayed on the right axis. The spectra have been translated vertically for display purposes.



Figure 7. A cartoon of how the change in packing density might affect the orientation of the fluorocarbon chains. The solid filled objects represent the molecules of **2** and the hatched objects represent DTBA molecules.

stretch (1533 cm^{-1}) and the CF_2 asymmetric stretch perpendicular to the fluorocarbon axis (1251 cm^{-1}). The intensities of these two bands decrease as a function of surface concentration of **2**. The Supporting Information shows that the nitro band decreases linearly with concentration; in contrast the CF_2 band initially increased in intensity before decreasing.

Given that vibrations parallel to the plane of the surface cannot be detected due to the “surface selection rule”, the initial increase of the fluorocarbon band would be consistent with a change in orientation of the semi-fluorinated chain with decreasing concentration of **2**; i.e., the fluorinated chains become increasingly tilted with decreasing concentration (Figure 7). Naselli et al. studied disorder transitions in Langmuir–Blodgett films of $[\text{CF}_3(\text{CF}_2)_8(\text{CH}_2)_{10}\text{COO}^-]_2\text{Cd}^+$ with elevated temperatures. It was noted that the fluorocarbon band at 1251 cm^{-1} increased with increasing temperatures, and it was proposed that was due to increasing tilt of the fluorocarbon chains.⁴⁶

Characterization of SAM1 and SAM2 Post UV Irradiation. SAM1 and SAM2 were irradiated using a 365 nm (7 mW/ cm^2) mercury lamp. Photolysis of SAM1 and SAM2 should leave SAMs with carboxylic acid groups present at the surface (Figure 1). Figure 4c shows the X-ray photoelectron C 1s spectra of SAM1 after 3600 s of UV irradiation. Clearly, there is large decrease in the relative amount of fluorocarbon to hydrocarbon species, which suggests that a large portion of the photocleavable groups have been removed by the exposure. The XPS of SAM2 after UV irradiation (Figure 4d) is similar to Figure 4c, indicating that the UV irradiation has modified both SAM1 and SAM2 in a similar manner. The FT-IR spectra of SAM1, before and after irradiation, are presented in Figure 5a. The first thing to note is that the band at 1533 cm^{-1} has almost disappeared. Second, the band at 1251 cm^{-1} has increased in intensity, and third, that the bands at $\sim 1740\text{ cm}^{-1}$ are still present after irradiation. This suggests that almost all of the nitro-groups have undergone either a photoreduction reaction or photocleavage reaction. A significant proportion of the semi-fluorinated moieties remain on the surface and must display a larger tilt angle (similar effect observed for the mixed SAMs). The spectra

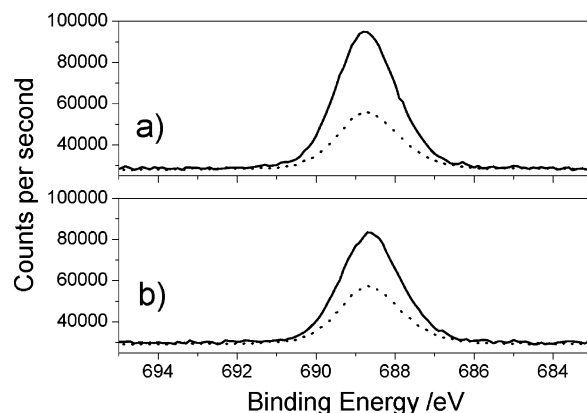


Figure 8. X-ray photoelectron spectra of the F 1s region; (a) SAM1 formed on Au; (b) SAM2 formed on Au. The dashed lines represent the F 1s signal after the SAMs had been treated for 3600 s of UV (365 nm, 7 mW/ cm^2) irradiation.

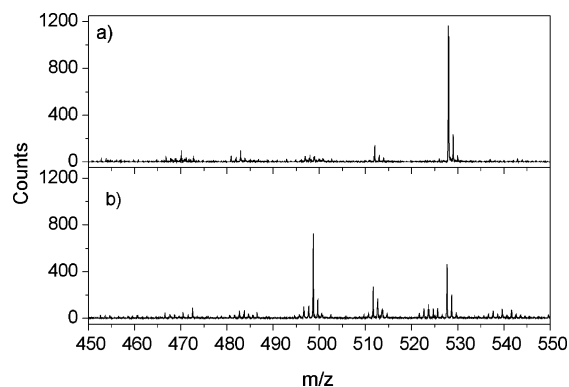


Figure 9. ToFSIMS of SAM2 (a) before UV irradiation and (b) after 3600 s of 365 nm UV irradiation.

obtained for SAM2 before, and after, irradiation is shown in Figure 5b. Similar conclusions can also be deduced from these spectra.

Figures 8a shows the F 1s regions of SAM1 before and after 3600 s UV irradiation, from which it can be estimated that 50% of the photocleavable moieties are removed from SAM1. Similarly, Figure 8b shows that $\sim 45\%$ of the photocleavable units in SAM2 were removed following the same irradiation. The yield of these reactions is significantly lower than those previously reported for SAM3.¹⁶ The reason for the difference in reaction yields between the systems may be related to (1) the packing density difference (SAM1 and SAM2 > SAM3) and (2) the spacing between the gold substrate and the *ortho*-nitro group is larger for SAM3 than SAM1 and SAM2. The ellipsometric thicknesses of SAM1 and SAM2 were measured after UV exposure, and these are summarized in Table 1. The thicknesses of SAM1 and SAM2 were reduced to 66% and 57% of their original film values, respectively.

To understand why the photoreaction yields were so low time-of-flight secondary ion mass spectroscopy (ToFSIMS) was used to analyze SAM2 before and after 3600 s of UV irradiation. A molecular weight that would correspond to the mass of an entire molecule from SAM2 was not observed. The main cleavage occurs, as expected, at the *O*-benzylic CH_2 bond position giving $m/z = 528$ $[\text{C}_{16}\text{H}_{11}\text{F}_{13}\text{O}_4\text{N}]^+$ (Figure 9a). Figure 9b shows the spectrum obtained from SAM2 after UV irradiation. This spectrum has peaks at m/z 498, 512, and 528. The peak at m/z 528 corresponds to unreacted molecules, that at m/z 498, $[\text{C}_{16}\text{H}_{14}\text{F}_{13}\text{O}_2\text{N}]^+$ corresponds to the reduction to amine ($\text{ArNO}_2 \rightarrow \text{ArNH}_2$) and that at m/z 512 to the nitroso compound (ArNO_2

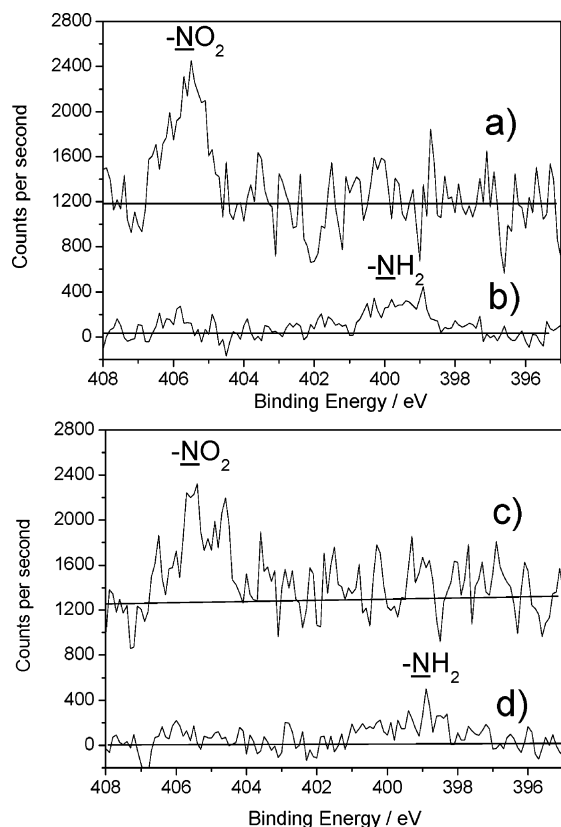


Figure 10. XPS of the N 1s region of (a) SAM1 before UV irradiation (b) after UV irradiation (c) and N 1s region of SAM2 before irradiation (d) and after UV irradiation. The spectra have been translated vertically for display purposes.

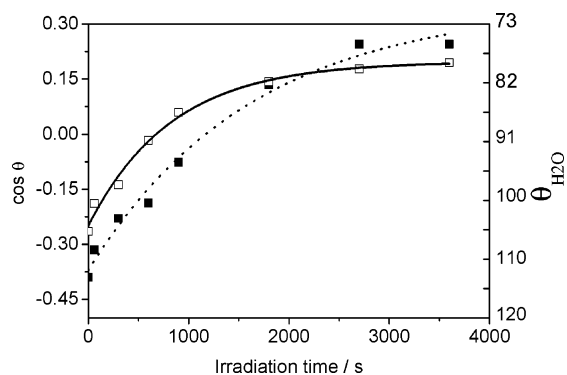


Figure 11. The variation of water contact angles, of SAM1 and SAM2, as a function of UV irradiation time. Symbols ■ and □ represent the mean of advancing and receding contact angles of SAM1 and SAM2, respectively. The lines are lines-of-best-fit of eq 3. The right axis is nonlinear.

→ ArNO) which is an intermediate in the reduction process. Furthermore, the XPS of the N 1s region of SAM1 and SAM2 shows evidence of the reduction of the nitro group (Figure 10). Initially, the N 1s band is centered at 405.5 eV this is close to the literature values for a nitro group.⁵⁰ These spectra were acquired rapidly to minimize the effects of X-ray reduction of the aromatic nitro group.⁵¹

Figure 11 displays the “average” ($\theta = (\theta_A + \theta_R)/2$) water contact angles as a function of irradiation time. The final values for the contact angles tend toward $\sim 80^\circ$, which is considerably higher than that expected for carboxylic acid functionalized SAMs. This is a further indication that the photoreactions are not 100% clean. Previous studies, of SAM3 showed that a fraction of the photocleavable groups could not be removed even

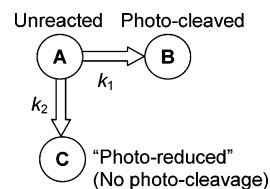


Figure 12. The photoreaction pathways: At any moment in time there will be a fraction of unreacted molecules, a fraction of photocleaved molecules and a fraction of photoreduced molecules (thereby removing a route for photocleavage). The rates of the reactions are given by k_1 and k_2 .

after extended irradiation times.¹⁶ Table 1 summarizes the contact angle data before and after 3600 s irradiation.

The XPS and SIMS results demonstrate that a competing photoreaction takes place; i.e., the photoreduction of a fraction of the nitro groups to amines occurs.^{16,20,52} Once the nitro group has been reduced there is no possibility of removing the hydrophobic moiety using soft UV light. So at any snapshot in time there will be a fraction of unreacted molecules, A; a fraction of photocleaved molecules, B; and a fraction of photoreduced (modified to become nonremovable) molecules, C (Figure 12).

The rate of decrease of unreacted molecules ($A \rightarrow B$ and $A \rightarrow C$) is assumed to be proportional to both the fraction of unreacted molecules and the number of photons striking the molecules per unit time. Similarly, the rate of “photocleavage” ($A \rightarrow B$), will also be proportional to the fraction of unreacted molecules and the number of photons striking the surface per unit time. These reaction rates can be presented in the form of two differentials that can be solved to give the fraction of hydrophobic moieties on the surface, ϕ , at any time, t ,

$$\phi = e^{-(k_1+k_2)t} + \frac{k_2}{k_1+k_2}[1 - e^{-(k_1+k_2)t}] \quad (1)$$

where, k_1 and k_2 are rate constants for the photocleavage and the competing side reaction, respectively. The constants can be written in a form to introduce a quantum efficiency term, η , so that

$$k_1 = \eta_1 \left(\frac{IA_m}{h\nu} \right) \text{ and } k_2 = \eta_2 \left(\frac{IA_m}{h\nu} \right) \quad (2)$$

Where I is the intensity of the light (units of W/m^2), A_m , is the area per molecule, and $h\nu$ is the photon energy. Equation 1 can be substituted into the Cassie⁵³ equation,

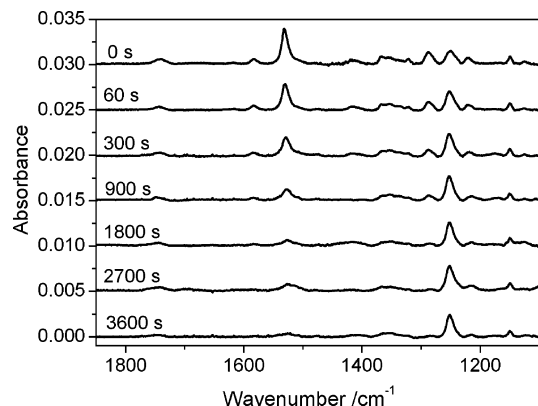
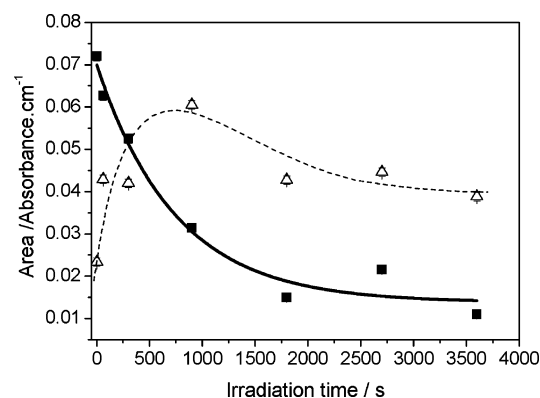
$$\cos\theta = \cos\theta_2 + \left(e^{-(k_1+k_2)t} + \frac{k_2}{k_1+k_2}[1 - e^{-(k_1+k_2)t}] \right) \times (\cos\theta_1 - \cos\theta_2) \quad (3)$$

where θ_1 is the contact angle of the surface at $t = 0$, and θ_2 is the contact angle of the surface if every molecule in the SAM underwent photocleavage (the final contact angle assuming 100% photocleavage). The Cassie equation should strictly only be applied to equilibrium contact angle data; so we have taken the average of the advancing and receding contact angles, i.e., $\theta = (\theta_A + \theta_R)/2$.

Equation 3 was fitted to the contact angle data in Figure 11, and Table 3 summarizes the constants, k_1 and k_2 , obtained. The quantum efficiencies of these reactions can be estimated from these constants using eq 2, given that the lower limit of average molecular cross-sectional area to be $2.9 \times 10^{-19} \text{ m}^2$ (assuming tightly packed semi-fluorinated chains³⁴), the light intensity to be 70 Wm^{-2} , and the average photon energy was 5.4×10^{-19}

TABLE 3: Summary of the Photoreaction Rate Constants and Estimated Quantum Efficiencies

SAM	$k_1 (\times 10^{-5} \text{ s}^{-1})$	$k_2 (\times 10^{-5} \text{ s}^{-1})$	$\eta_1 (\times 10^{-6})$	$\eta_2 (\times 10^{-6})$
SAM 1	33 ± 5	29 ± 1	9 ± 1	8 ± 2
SAM 2	44 ± 5	80 ± 10	11 ± 1	32 ± 3

**Figure 13.** FT-IR spectra of SAM2 as a function of irradiation time. The spectra have been translated vertically for display purposes.**Figure 14.** FT-IR determined peak areas versus irradiation time. The squares represent the NO₂ (1533 cm⁻¹) vibration and the triangles represent the CF₂ (1252 cm⁻¹) asymmetric stretch perpendicular to the chain axis. The solid line is a first-order exponential decay best fit through the NO₂ data and the dashed line is a guide-to-the-eye through the CF₂ data.

J. This gives the “photocleavage” quantum efficiency of SAM2 to be 33% larger than SAM1; however, one must exercise caution when considering this comparison since it is an oversimplification to assume that the packing densities are the same for SAM1 and SAM2 (given the data presented earlier). In the case of SAM1, the efficiency of the side reaction is close to that of the photocleavage reaction. In contrast the competing reaction rate of SAM2 was found to be almost twice the photocleaving reaction rate. This could be related to differences in separation between the nitro group and the substrate or differences in packing densities and hence orientation of the chromophore unit with respect to the surface normal.

FT-IR spectroscopy was also used to monitor SAM2 as a function of irradiation time (Figure 13). These data are similar to that seen for the FT-IR data of the mixed SAMs (Figure 6). The aromatic nitro band decreases with time, while the CF₂ asymmetric band at 1251 cm⁻¹ initially increases, before decreasing.

The integrated intensity of the bands has been plotted as a function of irradiation time and these are shown in Figure 14. The decrease in the intensity of the nitro band has two contributions: one due to the photocleavage reaction and the second associated with the “competing” side-reaction. The net

rate of decrease in intensity of this band will be $k_1 + k_2$, (assuming orientation effects are small). The line of best fit through these data gives $k_1 + k_2 = 1.3 \pm 0.1 \times 10^{-3} \text{ s}^{-1}$. This is similar to the value obtained from the contact angle data, $k_1 + k_2 = 1.2 \pm 0.1 \times 10^{-3} \text{ s}^{-1}$ (Table 3). The CF₂ band at 1251 cm⁻¹, however, initially increases over the first 1000 s, before decreasing. This suggests that the semi-fluorinated chains display increased tilt as the photolysis progresses (consistent with the mixed SAM model system). Comparison of the decrease in nitro band decreased from 0.072 to 0.014, with the mixed SAM systems corresponds to $\leq 30\%$ of the photocleavable (nitro containing) moieties remained on the surface. However, XPS data indicated that $\sim 55\%$ of the photocleavable units remained. This confirms that a fraction of the nitro groups must undergo a photoreaction, but that this reaction does not lead to the removal of the corresponding semi-fluorinated moiety.

Conclusions

This study shows both the advantages and disadvantages of this particular approach to functional group lithography of thiol-on-gold SAMs. The chemistry is simple, mild, and well-controlled and can be adapted easily to the production of CO₂H or NH₂ functionalized systems all of which (in principle) are capable of further chemical modification and elaboration. Indeed with this modular design of SAM the hydrophobic character, the photochemistry, and the functional group attachment can be almost independently modified and optimized.¹⁶ The disadvantages are that, compared to equivalent reactions in solution, the chemical yield is lower, the quantum efficiency is much lower and seen as a hydrophilic/hydrophobic switch system¹⁶ rather than a functional group switch system, and the recovery of hydrophilic character on photolysis is lower than would be expected on the basis of the chemical yield. The low quantum efficiency is not a serious practical problem since there is only a single molecular layer and the reactions are all quite rapid even with quite a low powered lamp. It presumably reflects quenching of the excited molecules by the gold. It also shows that the partitioning of the excited state molecules into various physical and chemical pathways is very different in the SAM to that experienced in solution. More disappointing are the relatively low chemical yield as compared to very similar reactions in dilute solution.^{17,19} In the case of the protected amine (SAM3) one possibility is that the side reaction involves imine formation,^{16,20} but it now seems unlikely that this is a significant factor. In particular, we note that the extent of side-reaction at the limit of the photolysis; the proportion of fluorinated moieties left bound to the surface is significant for SAM1, SAM2, and SAM3 systems suggesting that this is something inherent in the *ortho*-nitrobenzyl photochemistry. Indeed, the presence of a weak broad NH₂ signal in the XPS suggests that the problem is one of photoreduction. In the case of SAM2 this is confirmed by the SIMS evidence. Whereas photoreduction is perhaps the commonest of all photoreactions of aromatic nitro compounds,^{16,20,54} in general, intermolecular photoreduction is not a significant side reaction in the case of the *ortho*-nitrobenzyl protected systems. The fact that it is a significant competing process in the case of these *ortho*-nitrobenzyl protected SAMs is a reflection either of the close presence of the gold layer (a potential source of photoelectrons)⁵⁵ or of the close-packed nature of the SAMs (leading to a competition between intramolecular and intermolecular hydrogen atom abstraction by the photoexcited ArNO₂). The failure to recover the expected amount of hydrophilic character is only a problem if the aim is

to use this type of chemistry to create a hydrophobic/hydrophilic switch and the fact that, in the intermediate mixed SAMs, the long chain components tilt over and has a number of precedents and parallels in other systems.⁵⁶

Acknowledgment. We thank the Seiko-Epson Corporation for funding of this study. K.C. was also grateful to EPSRC for their financial support. We thank Dr Jean-Claude Canry and Dr Alan J. Paul for their help analyzing the ToFSIMS data.

Supporting Information Available: Details of synthesis of the photocleavable compounds. XPS determined surface concentration as a function of solution concentration for the mixed SAMs. Water contacts of the mixed SAMs. The nitro and CF₂ FT-IR bands of the mixed SAMs are plotted as a function of relative surface concentration of **2**. This material is available free of charge via the Internet at <http://pubs.acs.org>.

References and Notes

- (1) Dulcey, C. S.; Georger, J. H.; Krauthamer, V.; Stenger, D. A.; Fare, T. L.; Calvert, J. M. *Science* **1991**, *252*, 551–554.
- (2) Calvert, J. M.; Chen, M. S.; Dulcey, C. S.; Georger, J. H.; Peckerar, M. C.; Schnur, J. M.; Schoen, P. E. *J. Vac. Sci. Technol. B* **1991**, *9*, 3447–3450.
- (3) Dressick, W. J.; Calvert, J. M. *Jpn. J. Appl. Phys.* **1993**, *32*, 5829–5839.
- (4) Huang, J.; Hemminger, J. C. *J. Am. Chem. Soc.* **1993**, *115*, 3342–3343.
- (5) Huang, J. Y.; Dahlgren, D. A.; Hemminger, J. C. *Langmuir* **1994**, *10*, 626–628.
- (6) Georger, J. H.; Stenger, D. A.; Rudolph, A. S.; Hickman, J. J.; Dulcey, C. S.; Fare, T. L. *Thin Solid Films* **1992**, *210*, 716–719.
- (7) Tarlov, M. J.; Burgess, D. R. F.; Gillen, G. J. *Am. Chem. Soc.* **1993**, *115*, 5305–5306.
- (8) Brewer, N. J.; Rawsterne, R. E.; Kothari, S.; Leggett, G. J. *J. Am. Chem. Soc.* **2001**, *123*, 4089–4090.
- (9) Brewer, N. J.; Janusz, S.; Critchley, K.; Evans, S. D.; Leggett, G. J. *J. Phys. Chem. B* **2005**, *109*, 11247–11256.
- (10) Mendes, P. M.; Preece, J. A. *Curr. Opin. Colloid Interface Sci.* **2004**, *9*, 236–248.
- (11) Dressick, W. J.; Dulcey, C. S.; Chen, M. S.; Calvert, J. M. *Thin Solid Films* **1996**, *285*, 568–572.
- (12) Hong, L.; Sugimura, H.; Furukawa, T.; Takai, O. *Langmuir* **2003**, *19*, 1966–1969.
- (13) Alkhalifa, B.; Allinson, H.; Boden, N.; Evans, S. D.; Henderson, J. R. *Phys. Rev. E* **1999**, *59*, 3033–3039.
- (14) Ye, T.; McArthur, E. A.; Borguet, E. *J. Phys. Chem. B* **2005**, *109*, 9927–9938.
- (15) Ye, T.; Wynn, D.; Dudek, R.; Borguet, E. *Langmuir* **2001**, *17*, 4497–4500.
- (16) Critchley, K.; Jeyadevan, J. P.; Fukushima, H.; Ishida, M.; Shimoda, T.; Bushby, R. J.; Evans, S. D. *Langmuir* **2005**, *21*, 4554–4561.
- (17) Pillai, V. N. R. *Synthesis-Stuttgart* **1980**, 1–26.
- (18) Ryan, D.; Parviz, A. P.; Linder, V.; Semetey, V.; Sia, S. K.; Su, J.; Mrkich, M.; Whitesides, G. M. *Langmuir* **2004**, *20*, 9080–9088.
- (19) Bochet, C. G. *J. Chem. Soc., Perkin Trans. I* **2002**, 125–142.
- (20) Campo, A. d.; Boos, D.; Spiess, H. W.; Jonas, U. *Angew. Chem., Int. Ed.* **2005**, *44*, 4707–4712.
- (21) Zhao, B.; Moore, J. S.; Beebe, D. J. *Anal. Chem.* **2002**, *74*, 4259–4268.
- (22) Zhao, B.; Moore, J. S.; Beebe, D. J. *Langmuir* **2003**, *19*, 1873–1879.
- (23) Jonas, U.; del Campo, A.; Kruger, C.; Glasser, G.; Boos, D. *Proc. Nat. Acad. Sci. U.S.A.* **2002**, *99*, 5034–5039.
- (24) McGall, G. H.; Barone, A. D.; Diggelmann, M.; Fodor, S. P. A.; Gentalen, E.; Ngo, N. *J. Am. Chem. Soc.* **1997**, *119*, 5081–5090.
- (25) Nakagawa, M.; Ichimura, K. *Colloids Surf. A* **2002**, *204*, 1–7.
- (26) Jennane, J.; Boutros, T.; Giasson, R. *Can. J. Chem.* **1996**, *74*, 2509–2517.
- (27) Dunkin, I. R.; Gebicki, J.; Kiszka, M.; Sanin-Leira, D. *J. Chem. Soc., Perkin Trans. 2* **2001**, 1414–1425.
- (28) Yip, R. W.; Sharma, D. K.; Giasson, R.; Gravel, D. *J. Phys. Chem.* **1985**, *89*, 5328–5330.
- (29) Song, X.; Xu, C. R.; HT, H.; Siahaan, T. J. *Bioorganic Chem.* **2002**, *30*, 285–301.
- (30) Ichikawa, T.; Kitazaki, T.; Matsushita, Y.; Yamada, M.; Hayashi, R.; Yamaguchi, M.; Kiyota, Y.; Okonogi, K.; Itoh, K. *Chem. Pharm. Bull.* **2001**, *49*, 1102–1109.
- (31) Gangwar, S.; Pauletti, G. M.; Siahaan, T. J.; Stella, V. J.; Borchardt, R. T. *Org. Chem.* **1997**, *62*, 1356–1362.
- (32) Dugave, C. *J. Org. Chem.* **1995**, *60*, 601–607.
- (33) Tomkins, H. G. *A User's Guide to Ellipsometry*; Academic: New York, 1993.
- (34) Cheadle, E. M.; Batchelder, D. N.; Evans, S. D.; Zhang, H. L.; Fukushima, H.; Miyashita, S.; Graupe, M.; Puck, A.; Shmakova, O. E.; Colorado, R.; Lee, T. R. *Langmuir* **2001**, *17*, 6616–6621.
- (35) Laibinis, P. E.; Whitesides, G. M. *J. Am. Chem. Soc.* **1992**, *114*, 1990–1995.
- (36) Kulinich, S. A.; Farzaneh, M. *Surf. Sci.* **2004**, *573*, 379–390.
- (37) Fukushima, H.; Seki, S.; Nishikawa, T.; Takiguchi, H.; Tamada, K.; Abe, K.; Colorado, R.; Graupe, M.; Shmakova, O. E.; Lee, T. R. *J. Phys. Chem. B* **2000**, *104*, 7417–7423.
- (38) Ulman, A. *An Introduction to Ultrathin Organic Films From Langmuir-Blodgett to Self-Assembly*; Academic Press: Boston, 1991.
- (39) Beamson, G. G. *High Resolution XPS of Organic Polymers the Scienta ESCA300 Database G. Beamson and D. Briggs*; Wiley: Chichester, New York, 1992.
- (40) Perry, C. C.; Wagner, A. J.; Fairbrother, D. H. *Chem. Phys.* **2002**, *280*, 111–118.
- (41) Ohnishi, S.; Ishida, T.; Yaminsky, V. V.; Christenson, H. K. *Langmuir* **2000**, *16*, 2722–2730.
- (42) Briggs, D. *Practical Surface Analysis by Auger and X-ray Photoelectron Spectroscopy*; Wiley: Chichester, New York, 1983.
- (43) Bain, C. D.; Whitesides, G. M. *J. Phys. Chem.* **1989**, *93*, 1670–1673.
- (44) Debe, M. K. *Appl. Surf. Sci.* **1982**, *14*, 1–40.
- (45) Naselli, Swalen, J. D.; Rabolt, J. F. *J. Chem. Phys.* **1989**, *90*, 3855.
- (46) Chidsey, C. E. D.; Loiacono, D. N. *Langmuir* **1990**, *6*, 682–691.
- (47) Lenk, T. J.; Hallmark, V. M.; Hoffmann, C. L.; Rabolt, J. F. *Langmuir* **1994**, *10*, 4610–4617.
- (48) Kobayashi, M.; Sakashita, M.; Adachi, T. *Macromolecules* **1995**, *28*, 316–324.
- (49) Ulman, A. *Self-Assembled Monolayers of Thiols*; Academic Press: San Diego, 1998.
- (50) Nielsen, J. U.; Esplandiu, M. J.; Kolb, D. M. *Langmuir* **2001**, *17*, 3454–3459.
- (51) Mendes, P. M.; Belloni, M.; Hardy, C.; Nikitin, K.; Fitzmaurice, D.; Critchley, K.; Evans, S. D.; Preece, J. A. *ChemPhysChem.* **2003**, *4*, 884–889.
- (52) Han, S. W.; Lee, I.; Kim, K. *Langmuir* **2002**, *18*, 182–187.
- (53) Cassie, A. B. D. *Discuss. Faraday Soc.* **1948**, *3*, 11.
- (54) Barltrop; Coyle *Excited States in Organic Chemistry*; Wiley: New York, 1975.
- (55) Kim, E.; Lee, I. *Langmuir* **2004**, *20*, 7351–7354.
- (56) Ionita, P.; Caragheorgheopol, A.; Gilbert, B. C.; Chechik, V. J. *Phys. Chem. B* **2005**, *109*, 3734–3742.